Supporting Information

Polymersomes with Aggregation-Induced Emission Based on Amphiphilic Block Copolypeptoids

Xinfeng Tao[1,2], Hui Chen[2], Sylvain Trépout[5], Jiayu Cen[3], Jun Ling[3], Min-Hui Li*[2,4]

[1] Shanghai Key Laboratory of Advanced Polymeric Materials, School of Materials Science and Engineering, East China University of Science and Technology, Shanghai 200237, China

[2] Chimie ParisTech, PSL Université Paris, CNRS, Institut de Recherche de Chimie Paris, UMR8247, 11 rue Pierre et Marie Curie, 75005 Paris, France.

[3] MOE Key Laboratory of Macromolecular Synthesis and Functionalization, Department of Polymer Science and Engineering, Zhejiang University, Hangzhou 310027, China

[4] Beijing Advanced Innovation Center for Soft Matter Science and Engineering, Beijing University of Chemical Technology, 15 North Third Ring Road, Chaoyang District, 100029 Beijing, China.

[5] Institut Curie, PSL Université Paris, INSERM U1196 and CNRS UMR9187, 91405 Orsay cedex, France

* Correspondence to: Min-Hui Li (E-mail: min-hui.li@chimieparistech.psl.eu)

1. Materials

Sarcosine (98%, Sigma-Aldrich), potassium ethylxanthate (>90%, TCI), sodium chloroacetate (98%, Sigma-Aldrich), phosphorus tribromide (PBr_3, 99%, Sigma-Aldrich), *N*-allylamine (98%, Sigma-Aldrich), glyoxylic acid (50 wt% aqueous solution, Alfa Aesar), mercaptoacetic acid (99%, Acros), 2-mercaptoethanol (>98%, TCI), benzyl mercaptan (>96%, TCI), 3-bromo-1-propanol (97%, Alfa Aesar), potassium carbonate (K_2CO_3, 99%, Sigma-Aldrich), sodium hydroxide (NaOH, 99%, VWR), magnesium sulfate ($MgSO_4$, dry, 98%, VWR), methanol (99%, VWR), diethyl ether (99%, VWR), chloroform (99%, VWR), hydrochloric acid (HCl, 37 wt% aqueous solution, VWR), ethyl acetate (99%, VWR) and petroleum ether (boiling point 40−60 °C, VWR) were used as received. Benzylamine (99%, Sigma-Aldrich) was stirred over CaH_2 (95%, Sigma-Aldrich) followed by distillation under vacuum. Acetonitrile (99%, VWR) was dried by CaH_2 and distilled.

2. Instruments and measurements

2.1 Size exclusion chromatography (SEC)

The number-average molecular weights (M_n) and molecular weight distributions of polymers (polydispersity index, PDI) were determined by size-exclusion chromatography (SEC) on a PL-50 (Agilent) system with two Mixed-C columns. DMF containing 0.02 mol/L LiBr was used as eluent with a flow rate of 1.0 mL/min. The temperature of the columns and RI detector was set as 50 °C. Commercial monodisperse polystyrenes were used as calibration standards.

2.2 Nuclear magnetic resonance (NMR)

Nuclear magnetic resonance (NMR) spectra were recorded on a Bruker Avance DMX 400 spectrometer (^{1}H: 400 MHz and ^{13}C: 100 MHz) with DMSO-d_6 or $CDCl_3$ as solvents and tetramethylsilane (TMS) as internal reference.

2.3 Matrix-assisted laser desorption/ionization time-of-flight mass spectrometer

(MALDI-ToF MS)

MALDI-ToF MS spectra were collected on a Bruker UltraFLEX MALDI-ToF mass spectrometer in the reflector mode. 2,5-Dihydroxybenzoic acid (DHB) was used as matrices, and potassium trifluoroacetate was used as the cationic agent. The nitrogen laser wavelength was set at 337 nm with a pulse interval of 3 ns. The acceleration voltage was set at 20 kV in reflection mode.

2.4 UV-vis absorption and Fluorescence spectroscopy

UV-vis absorption spectra were measured on a PerkinElmer Lambda 800 spectrometer. Photoluminescence (PL) spectra were recorded on a Spex FluoroMax Spectrofluorometer. For both UV-vis absorption spectra and PL spectra sample solutions with concentrations of approximately 10^{-5} M were placed in quartz cells with a path length of 1 cm.

2.5 Fluorescent quantum yield (QY)

The absolute fluorescent quantum yields of the nanoparticles were measured by integrated sphere on a QM-40 spectrofluorometer (PTI, Horiba) equipped with a 150 W xenon lamp. The excitation wavelength was set as 360 nm, and QY measurement was repeated for three times for each sample.

2.6 Dynamic light scattering (DLS)

Average diameters (D_h) of nanoparticles of P(TPE-NAG)-*b*-PSar block copolymers and their size distributions in deionized water were measured at 25 °C by dynamic light scattering (DLS, Malvern zetasizer Nano-ZS90) with a 633 nm laser. A 90° scattering angle was used for all measurements.

2.7 Cryo-electron microscopy (Cryo-EM)

Cryo-EM images were acquired on a JEOL 2200FS energy-filtered (20 eV slit) field emission gun electron microscope operating at 200 kV using a Gatan ssCCD

2048 × 2048 pixels. For the sample preparation, a total of 5 μL of samples were deposited onto a 200-mesh holey copper grid (Ted Pella Inc., U.S.A.) and flash-frozen in liquid ethane cooled down at liquid nitrogen temperature using a Leica CPC system.

2.8 Transmission electron microscopy (TEM)

TEM images were obtained using a HITACHI HT7700 instrument. A drop of nanoparticle solution in water was added onto the carbon film and followed by a drop of 2% phosphotungstic acid solution. The carbon film was dried under ambient conditions before TEM analysis.

3. Synthesis and characterization of NNTA monomers

3.1 Synthesis of Sar-NTA

Sar-NTA was synthesized according to our previous report as shown in Scheme S1.[1] The structure of Sar-NTA was well characterized by ^{1}H NMR spectrum as shown in Figure S1.

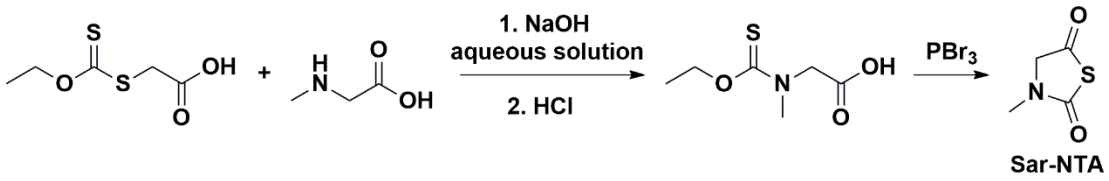

Scheme S1. Synthesis of Sar-NTA.

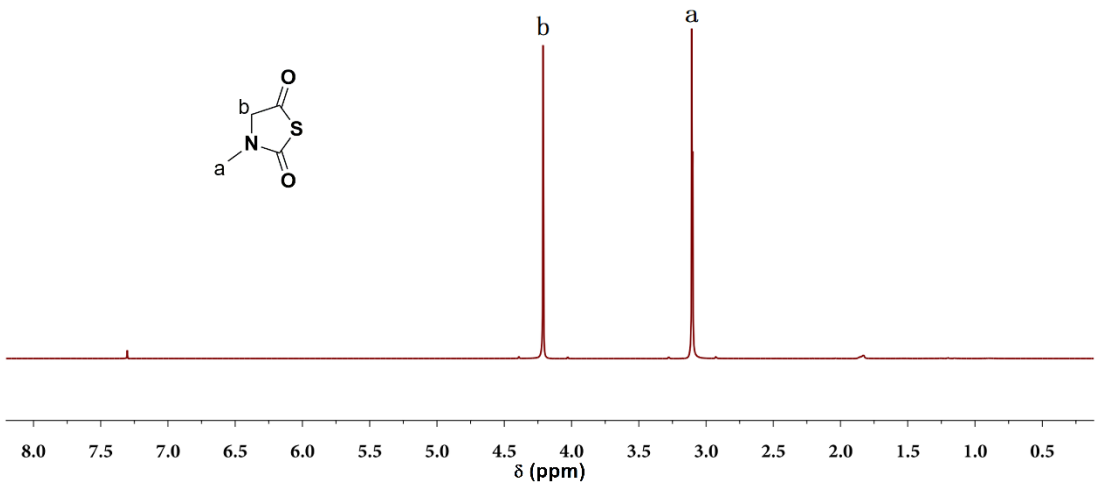

Figure S1. ^{1}H NMR spectrum of Sar-NTA in $CDCl_3$.

3.2 Synthesis of *N*-Allylglycine Hydrochloride.

N-Allylglycine hydrochloride was synthesized according to the literature (Scheme S2 and Figure S2).[2] 50 wt% aqueous solution of glyoxylic acid (107.84 g, 0.728 mol) and allylamine (19.51 g, 0.342 mol) were added to 500 mL H_2O. After stirred at r.t. for 24 h, 10 M hydrochloric acid (200 mL) was added. The reaction mixture was refluxed for 24 h. Then the solvent was concentrated. The yellow crude product was recrystallized in methanol/acetone to obtain white crystals (33.11 g, yield 63.9%). ^{1}H NMR (DMSO-d_6/TMS) δ: 3.57 ppm (d, 2H), 3.79 ppm (s, 2H), 5.43 ppm (q, 2H), 5.93 ppm (m, 1H), 9.55 ppm (s, 2H).

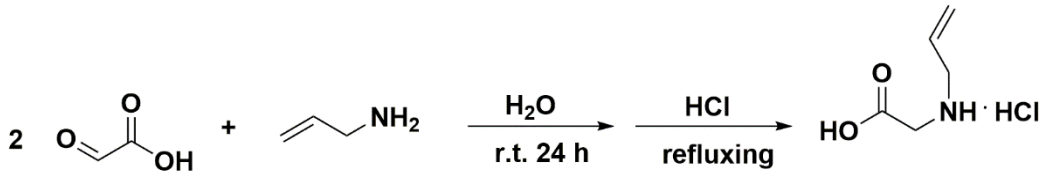

Scheme S2. Synthesis of *N*-allylglycine hydrochloride.

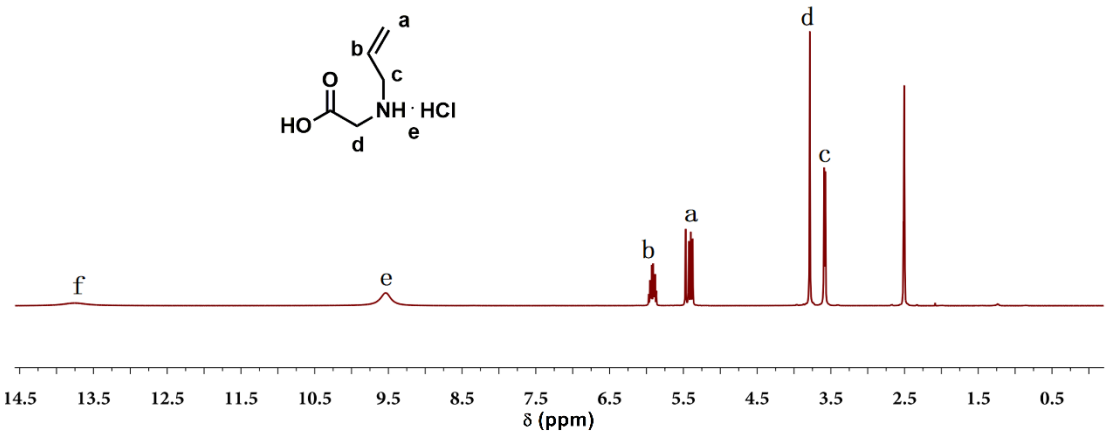

Figure S2. ^{1}H NMR spectrum of *N*-allylglycine hydrochloride in DMSO-d_6.

3.3 Synthesis of NAG-NTA

NAG-NTA was synthesized by the same procedure of other NNTAs reported by us (Scheme S3).[2] NaOH (24.36 g, 0.609 mol), *S*-ethoxythiocarbonyl mercaptoacetic acid[1] (36.59 g, 0.203 mol) and *N*-allylglycine hydrochloride (30.77 g, 0.203 mol) were dissolved in 300 mL water and allowed to stir for 72 h at 25 °C. Then the reaction mixture was acidified with concentrated hydrochloric acid to pH ~ 1 and extracted with chloroform. The extracts were washed with aqueous citric acid (5 wt%),

dried with $MgSO_4$, and concentrated under reduced pressure. The product *N*-ethoxythiocarbonyl-*N*-allylglycine was dissolved in 200 mL dry chloroform in an argon atmosphere. PBr_3 (19.5 mL, 0.205 mol) was added dropwise with stirring in an ice-water bath in 5 min. The reaction mixture was stirred for 10 more minutes at 0 °C and 1 h at room temperature. After washed with saturated solution of $NaHCO_3$ and deionized water, the chloroform solution was dried with $MgSO_4$ and concentrated in vacuum. The crude product was purified by column chromatography (ethyl acetate : petroleum ether = 1:8). Yellow oil was obtained (9.01 g, yield 28.2%) and stored under argon atmosphere. ^{1}H NMR ($CDCl_3$/TMS) δ: 4.14 ppm (d, 2H), 4.16 ppm (s, 2H), 5.31 ppm (q, 2H), 5.80 ppm (m, 1H). ^{13}C NMR ($CDCl_3$/TMS) δ: 46.57 ppm (CH_2=CH*C*H_2-), 59.18 ppm (-*C*H_2CO-), 120.10 ppm (*C*H_2=CHCH_2-), 130.20 ppm (CH_2=*C*HCH_2-), 164.77 ppm (-N*C*OSCO-), 194.07 (-NCOS*C*O-).

The structures of NAG-NTA was well characterized by NMR spectra (Figure S3-S6). For NAG-NTA the signal of vinyl protons of allyl side group is found at 5.31 ppm (q, H^a) and 5.80 ppm (m, H^b), and methylene protons on side group appear at 4.14 ppm (d, H^c). The signal at 4.16 ppm (s, H^d) is assigned to methylene protons on five-membered ring (Figure S3). The vinyl signal H^b is coupled with signal H^a and H^c, respectively (insert A and B in Figure S5). ESI-MS spectrometry of NAG-NTA shows a peak at 158.0261 m/z generated by [(NAG-NTA)H^+] (theoretical value: 158.0276 m/z).

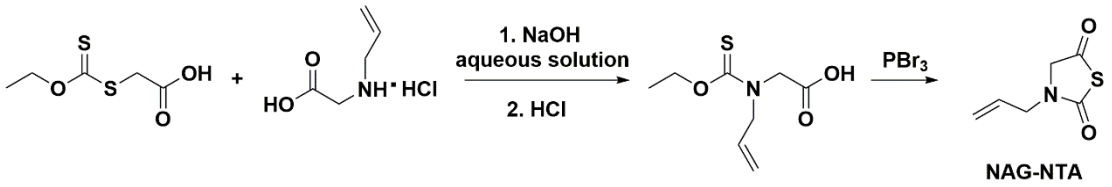

Scheme S3. Synthesis of NAG-NTA.

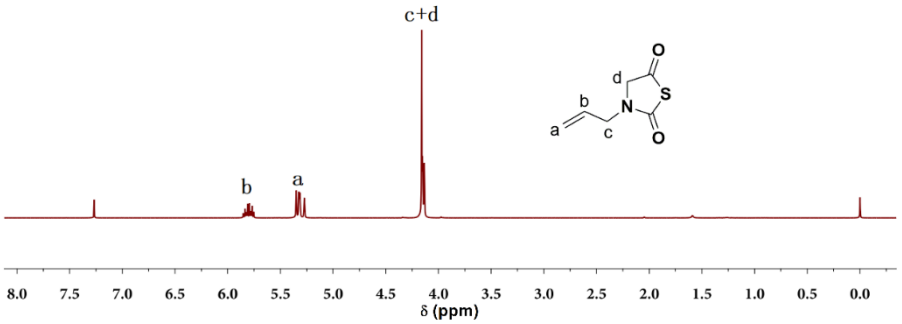

Figure S3. ^{1}H NMR spectrum of NAG-NTA in $CDCl_3$.

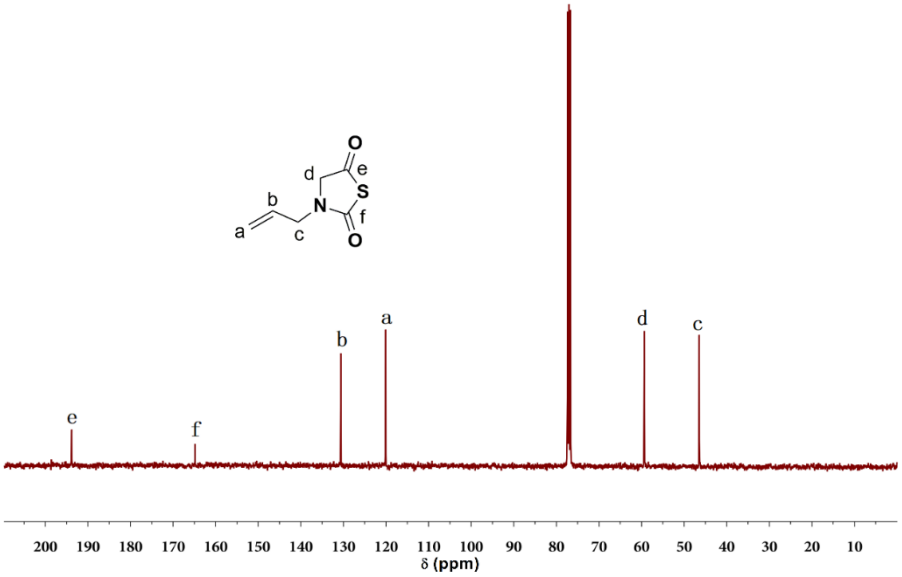

Figure S4. ^{13}C NMR spectrum of NAG-NTA in $CDCl_3$.

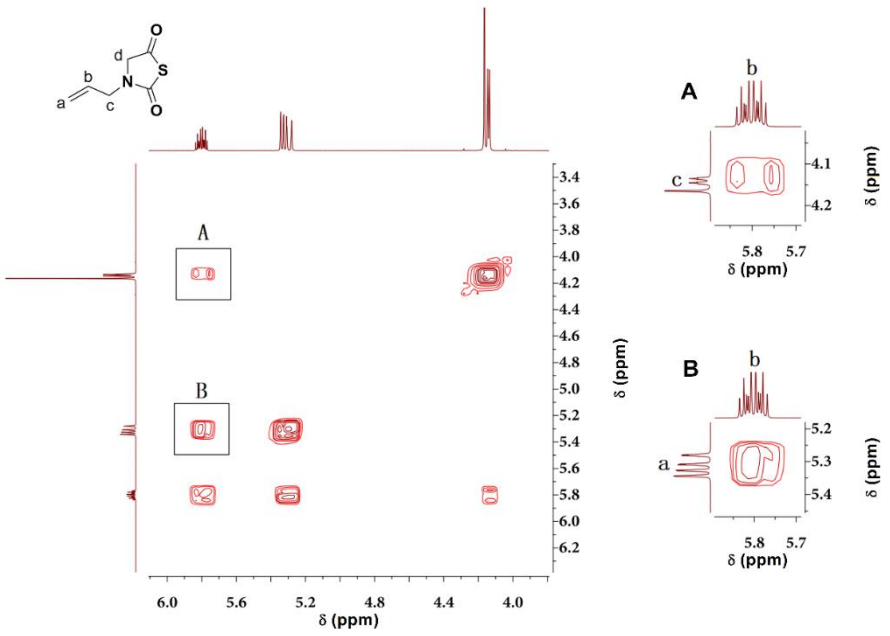

Figure S5. ^{1}H-^{1}H COSY spectrum of NAG-NTA in $CDCl_3$.

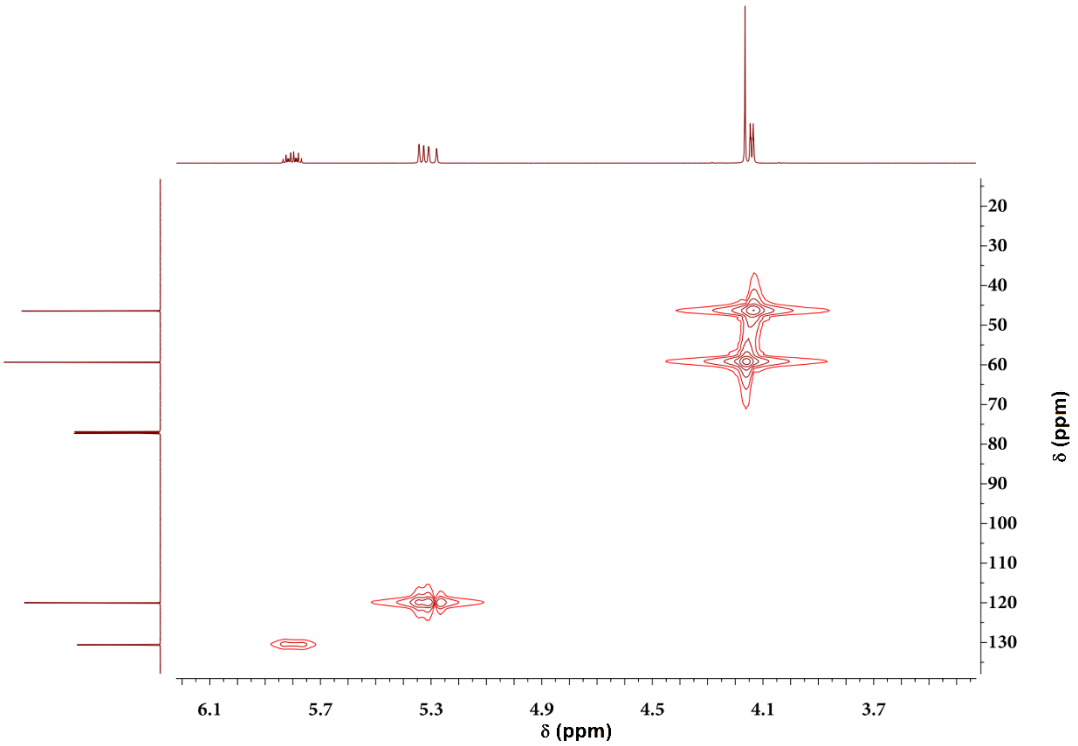

Figure S6. ^{1}H-^{13}C HMQC spectrum of NAG-NTA in $CDCl_3$.

4. Synthesis of 3-(4-(1,2,2-triphenylvinyl)phenoxy)propan-1-ol (TPE-C_3OH)

Potassium carbonate (2.65 g, 19.17 mmol) was added to a solution of 4-(1,2,2-triphenylvinyl)phenol[3] (2.10 g, 6.03 mmol) and 3-bromo-1-propanol (0.69 g, 4.98 mmol) in anhydrous DMF (45 mL). The reaction mixture was stirred at 90 ^{o}C for 6 h and then at 105 ^{o}C for 1 h. After filtration of the precipitate, the solvent was removed by evaporation. The residue was purified on silica gel using column chromatography with a dichloromethane and ethyl acetate (20:1) mixture as the eluent, giving the desired product as light yellow solid: 1.32 g (65.3%).[4] ^{1}H NMR ($CDCl_3$): 6.59-7.18 ppm (Ar, 19H), 4.05 ppm (t, 2H), 3.84 ppm (t, 2H), 2.00 ppm (m, 2H).

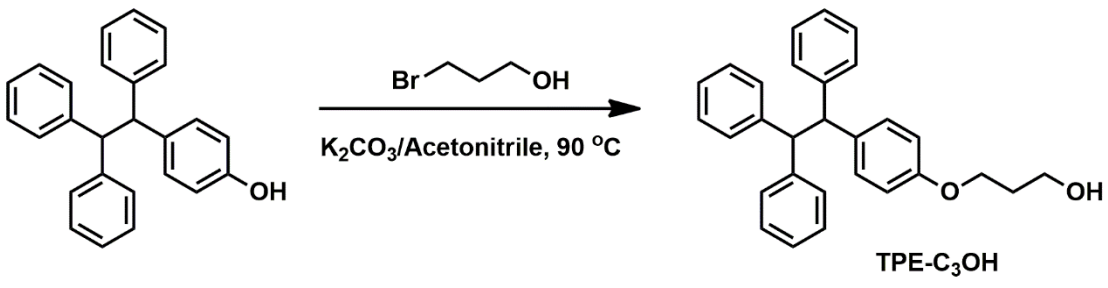

Scheme S4. Synthesis of TPE-C_3OH.

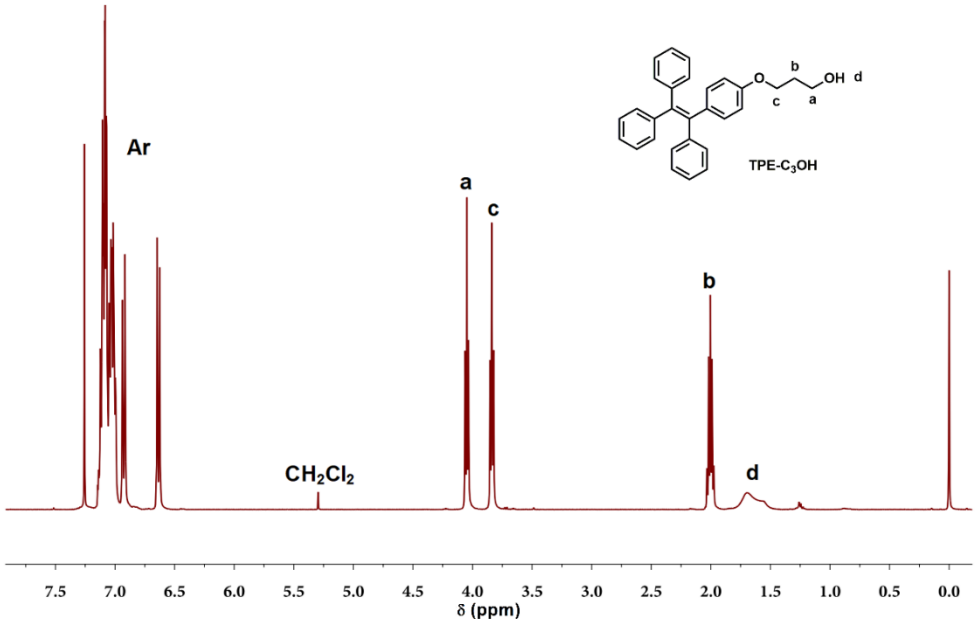

Figure S7. ^{1}H NMR spectrum of TEP-C_3OH in $CDCl_3$.

5. Polymerization of NAG-NTA and side-chain functionalization of PNAG

5.1 Polymerization of NAG-NTA

Table S1. Synthesis and characterization of PNAG, and PNAG-*b*-PSar[a]

Polymer Sample[b]	[NAG]/[Sar] /[I]	Time (h)	Conversion[c] (%)	$M_{n\ NMR}$[b] (kg/mol)	$Đ$[d]
$PNAG_{10}$	10/0/1	24	100	1.1	-[e]
$PNAG_{15}$	15/0/1	24	100	1.6	-[e]
$PNAG_{25}$	25/0/1	24	100	2.5	1.10
$PNAG_{50}$	50/0/1	48	100	3.6	1.10
$PNAG_{77}$	75/0/1	48	100	5.0	1.09
$PNAG_{10}$-*b*-$PSar_{53}$	10/50/1	24+36	93.0[f]	4.8	1.09
$PNAG_{15}$-*b*-$PSar_{54}$	15/50/1	24+36	88.1[f]	5.4	1.14
$PNAG_{25}$-*b*-$PSar_{46}$	25/50/1	24+36	86.3[f]	5.8	1.12

[a] Polymerizations were carried out at 60 °C with $[M]_0$ = 0.5 mol/L. [b] The degrees of polymerization (DP) and molecular weights of all polymers were determined by NMR. For example, DP = 10 in $PNAG_{10}$. [c] By taking a small amount of reaction mixture and dissolving in DMSO-d_6 for ^{1}H NMR analysis, monomer conversions were calculated from the relative integration of the proton resonance of monomers and copolymers. [d] Determined by SEC. [e] The molecular weight is too low to be determined by SEC. [f] Isolated yield after purification.

Benzylamine-initiated homopolymerizations of NAG-NTA were carried out in acetonitrile at 60 °C with various feed molar ratios changing from 10 to 75 (Table S1). As a typical homopolymerizations, NAG-NTA (0.349 g, 2.22 mmol) was dissolved in 4.0 mL dry acetonitrile, followed by 0.47 mL benzylamine in acetonitrile solution (0.1965 mol/L). The tube was sealed and placed in a 60 °C oil bath for 24 h. The polymer was isolated by precipitation from diethyl ether and dried in vacuum (0.219 g, 97.2%).

Quantitative complete monomer conversion was achieved in 24 h when the feed molar ratios of [NAG]/[I] were below 25, while 48 hours was needed for the full consumption of monomer when [NAG]/[I] = 50 or 75. Under the same reaction conditions, the polymerization of Sar-NTA and *N*-ethylglycine NTA (NEG-NTA) with 100% of conversion needed less time as we reported previously.[2] It meant that compared to Sar-NTA and NEG-NTA, NAG-NTA had a lower polymerization rate, similar to the low polymerization rate of *N*-allylglycine NCA (NAG-NCA),[5] which was caused by the steric and electronic properties of allyl side group. The MALDI-ToF mass spectrum of poly(*N*-allylglycine) (PNAG) shows a monomodal and symmetrical distribution (Figure S8). It reveals every polymer chain has benzyl and amino end groups, which is in conformity with normal amine mechanism (NAM).[2, 6] All signals of PNAG protons are definitely assigned in ^{1}H NMR spectrum as reported (Figure S9A).[7, 8] The degree of polymerization (DP) of the obtained PNAGs calculated from ^{1}H NMR according to signals H^{a} and H^{f} agrees well with the theoretical ones ([NAG]/[I]) in all polymerizations, which demonstrates the well-controlled characteristic of NAG-NTA polymerizations based on single-site initiation by benzylamine. The SEC traces (Figure S10) of PNAGs are monomodal with low polydispersity indexes ($Đ$ < 1.10). The small shoulders at tail positions of high molecular weights (MW) in SEC traces are attributed to non-optimized SEC conditions and possible polymer aggregations in solvents,[2, 9, 10] similar to the case of NAG-NCA polymerization.[8] Indeed, the monomodal and symmetrical mass spectrum without shoulders was actually observed by MALDI-ToF (Figure S8).

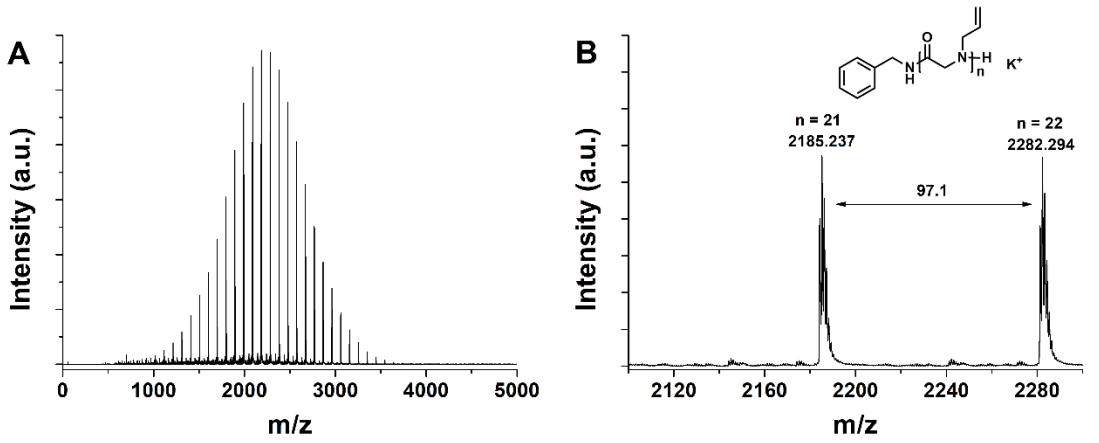

Figure S8. MALDI-ToF mass spectra of $PNAG_{25}$ (A) with zoom-in views and the corresponding polypeptoid structures (B).

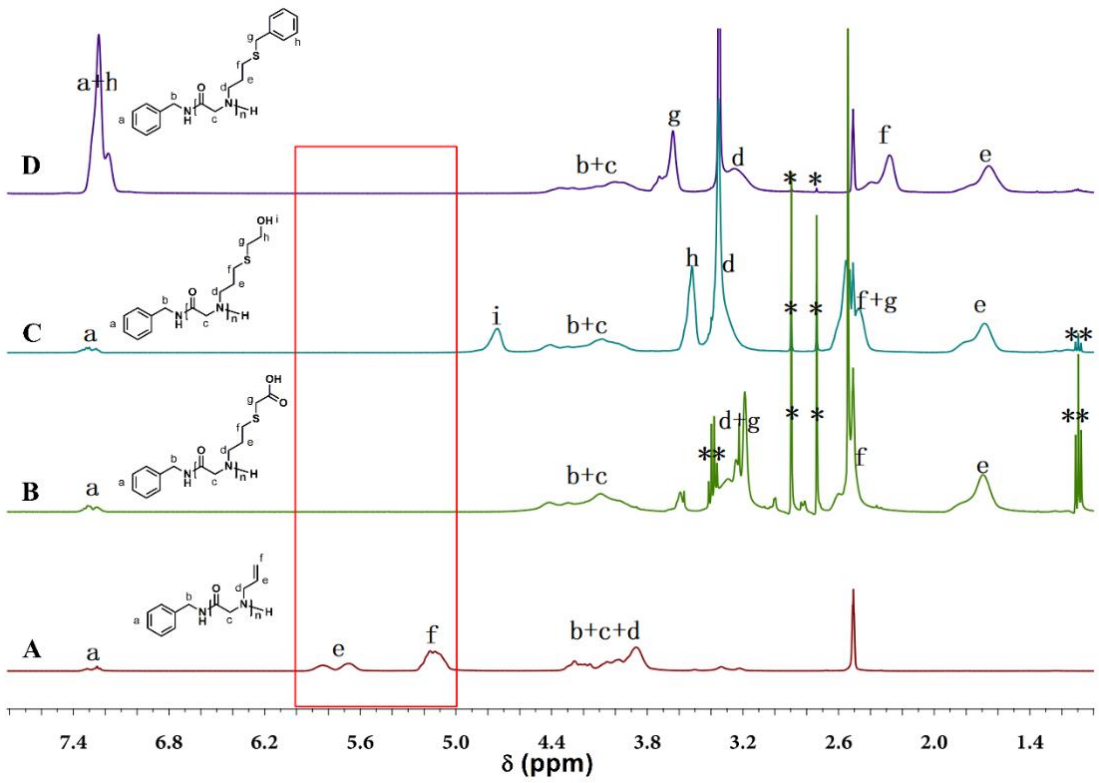

Figure S9. ^{1}H NMR spectra of (A) $PNAG_{25}$ and its corresponding products modified with (B) mercaptoacetic acid, (C) mercaptoethanol and (D) benzyl mercaptane in DMSO-d_6 (*: N,N-dimethylformide; **: diethyl ether).

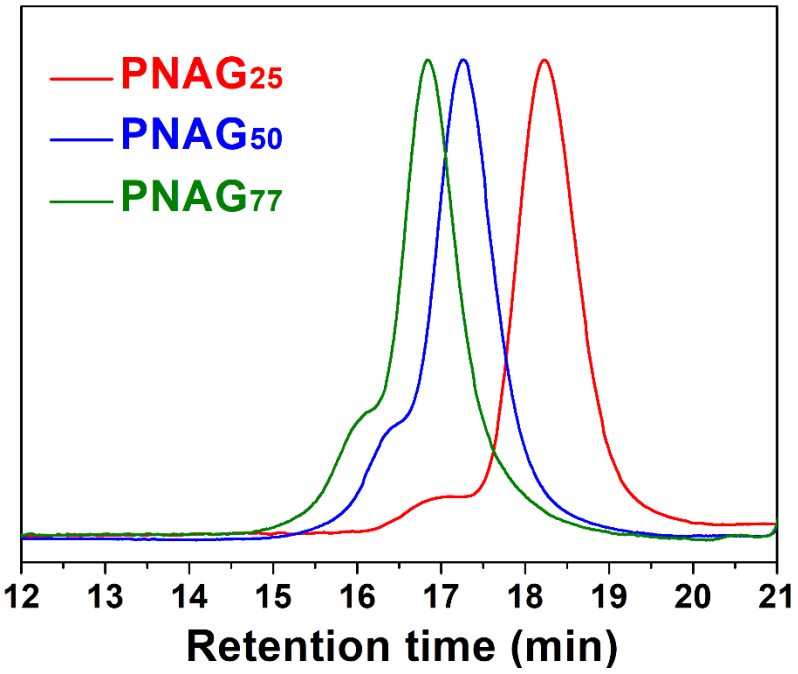

Figure S10. SEC traces of $PNAG_{25}$, $PNAG_{50}$ and $PNAG_{77}$.

5.2 Side-chain functionalization of PNAG

Mercaptoacetic acid, mercaptoethanol, and benzyl mercaptan were selected as the model compounds for the side chain modification (Scheme S5). As an example, $PNAG_{25}$ (51.8 mg, [allyl] = 0.511 mmol), mercaptoacetic acid (0.953 g, 10.35 mmol), and 2,2'-azobis(2-methylpropionitrile) (AIBN) (17.8 mg, 0.108 mmol) were dissolved in 3.0 mL DMF and deoxygenated by three freeze-pump-thaw cycles, sealed, and reacted at 60 °C for 24 h. Carboxylic acid functionalized polypeptoid $P(CA\text{-}NAG)_{25}$ was isolated by precipitation from diethyl ether and dried in vacuum (68.9 mg, 69.7%).

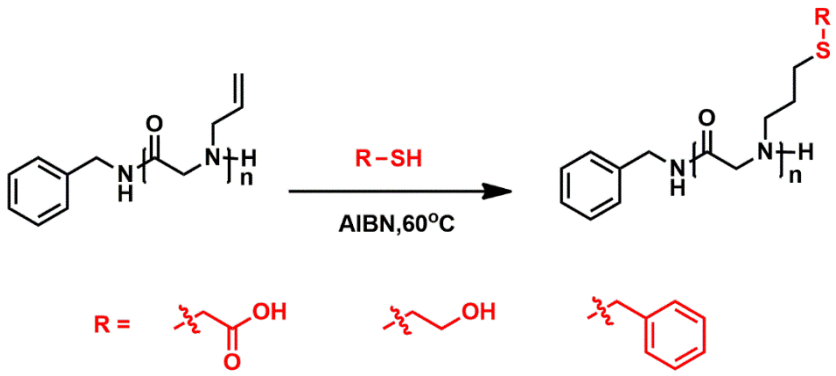

Scheme S5. PNAG side chain modifications by mercaptoacetic acid, mercaptoethanol, and benzyl mercaptan as the model compounds.

6. Synthesis and characterization PNAG-*b*-PSar

Taking advantages of living characteristic of primary amine-initiated NNTA polymerization, block copolypeptoids can be synthesized by sequential feeding of different monomers.[2] PNAG-*b*-PSar with three different molecular weights (Table S1) were then synthesized by sequential feeding of different amount of NAG-NTA and Sar-NTA initiated by benzylamine in acetonitrile at 60 °C (Scheme 1). As a typical block copolymerization, NAG-NTA (0.510 g, 3.24 mmol) was dissolved in 60 mL dry acetonitrile, followed by 0.61 mL benzylamine in acetonitrile solution (0.2111 mol/L). The tube was sealed and placed in a 60 °C oil bath. After 24 h, NAG-NTA was consumed (confirmed by ^{1}H NMR analysis), and 3.2 mL solution was removed from the reaction mixture for the analytical investigations of the first block. Then Sar-NTA (0.412, 3.14 mmol) was added to the reaction mixture of the first block. Additional 36 h the reaction mixture was stirred. The polymer was isolated by precipitation from diethyl ether and dried in vacuum (0.337 g, 86.3%).

All the block copolypeptoids were produced with high yields (> 86%). SEC traces with narrow distribution ($Đ$ < 1.14) (Figure S11) reveal that MW increases from the first block to the corresponding block copolymer. Protons of both NAG and Sar units are observed in ^{1}H NMR spectra of the final products (Figure 1A). The chain length of the block copolymers can be precisely controlled by the feed molar ratios according to the calculation of NMR. All the above results prove the successful synthesis of PNAG-*b*-PSar. Accordingly, the compositions of the three diblock copolypeptoids are calculated as $PNAG_{10}$-*b*-$PSar_{53}$, $PNAG_{15}$-*b*-$PSar_{54}$ and $PNAG_{25}$-*b*-$PSar_{46}$. Herein, PSar is the hydrophilic block with comparable protein resistance like PEG and minimal non-specific interactions with the biological environment, which is appropriate for the biomedical applications;[11] PNAG with allyl side groups is excellent platform for the further modification to get functional hydrophobic blocks, for instance, polypeptoids with AIE properties (Scheme 1).

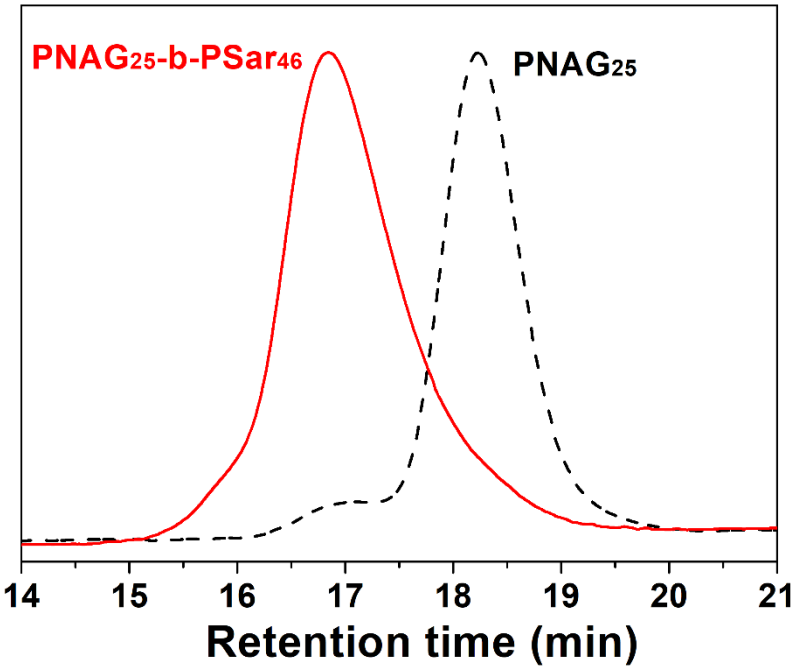

Figure S11. SEC traces of $PNAG_{25}$ and $PNAG_{25}$-*b*-$PSar_{46}$.

7. Synthesis and characterization P(TPE-NAG)-*b*-PSar

PNAG-*b*-PSar reacted with mercaptoacetic acid (CA-SH) in DMF at 60 °C for 24 h in the presence of AIBN through the radical-addition of thiol and allyl groups. The quantitative reaction of allyl groups was proved by the disappearance of vinyl proton signals at 5.0-6.0 ppm in ^{1}H NMR spectrum (Figure 1B), and carboxylic acid-functionalized P(CA-NAG)-*b*-PSar was obtained. As an example, $PNAG_{25}$-*b*-$PSar_{46}$ (40 mg, [allyl] = 0.172 mmol), mercaptoacetic acid (0.324 g, 3.52 mmol), and 2,2'-azobis(2-methylpropionitrile) (AIBN) (6.0 mg, 0.036 mmol) were dissolved in 2.5 mL DMF and deoxygenated by three freeze-pump-thaw cycles, sealed, and reacted at 60 °C for 24 h. Carboxylic acid functionalized copolypeptoids $P(CA\text{-}NAG)_{25}$-*b*-$PSar_{46}$ was isolated by precipitation from diethyl ether and dried in vacuum (54.4 mg, 92.5%).

Then condensation reaction between TPE-C_3OH (see Scheme S4 and Figure S7) and carboxylic groups on P(CA-NAG)-*b*-PSar was conducted at room temperature for 24 h in the presence of 4-dimethylaminopyridine (DMAP) and dicyclohexylcarbodiimide (DCC). As an example, $P(CA\text{-}NAG)_{25}$-*b*-$PSar_{46}$ (38.4 mg,

[carboxylic acid] = 0.118 mmol), TPE-C_3OH (0.271 g, 0.667 mmol), DCC (0.131 g, 0.635 mmol) and DMAP (0.016 g, 0.131 mmol) were dissolved in 3.0 mL DMF, and reacted at room temperature for 24 h. DMF was removed under vacuum, the solid residue was dissolved in CH_2Cl_2 and filtrated by Teflon filter. P(TPE-NAG)$_{25}$-*b*-PSar$_{46}$ was isolated by precipitating filtrate in diethyl ether and dried in vacuum (63.2 mg, 74.9%).

All the side chains of PNAG were attached with TPE groups according to the integral of benzylamine protons (H^a) and TPE protons (H^b) in Figure S12. SEC trace of P(TPE-NAG)-*b*-PSar showed the increasing of MW compared to the one of PNAG-*b*-PSar (Figure S13).

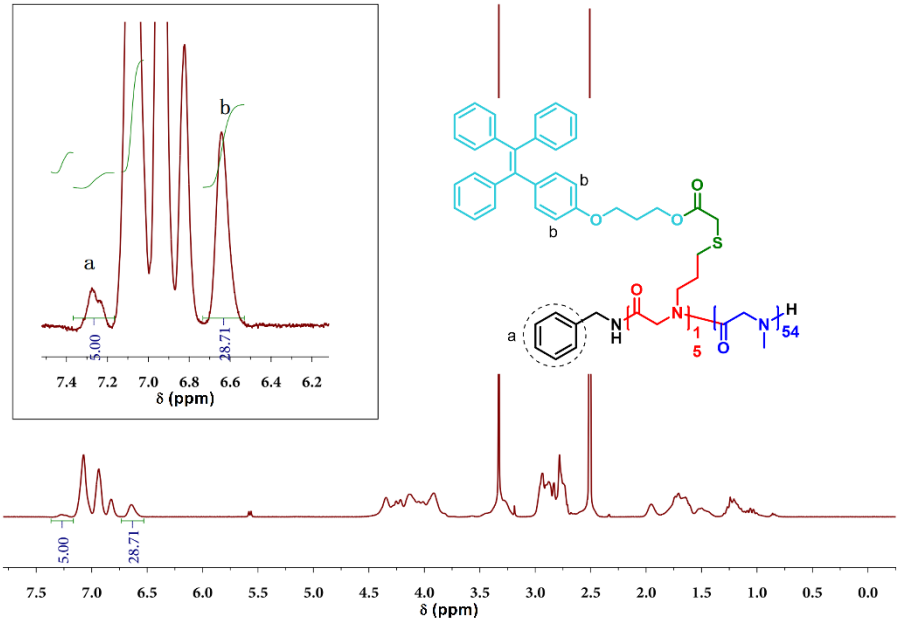

Figure S12. ^{1}H NMR spectra of P(TPE-NAG)$_{15}$-*b*-PSar$_{54}$ in DMSO-d_6.

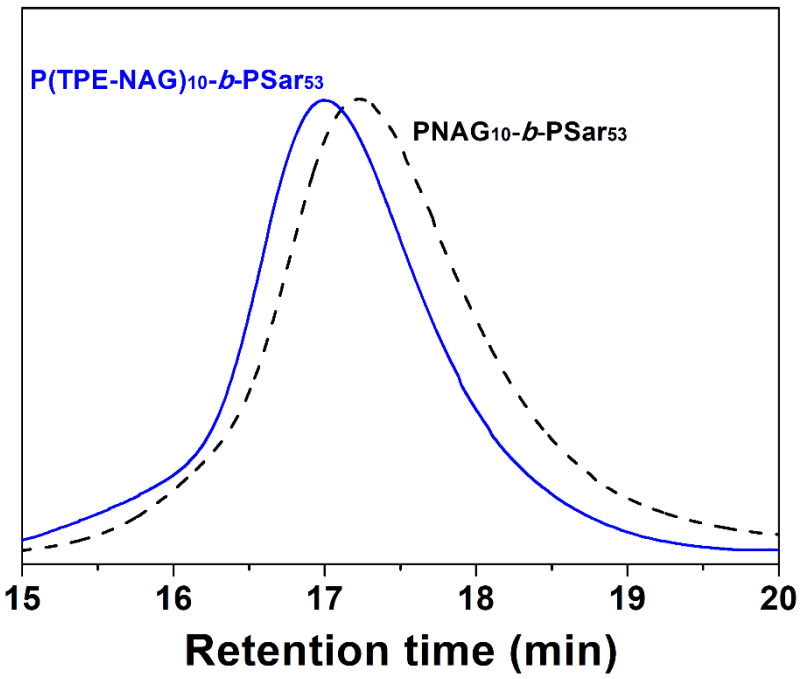

Figure S13. SEC traces of $PNAG_{10}$-*b*-$PSar_{53}$ and $P(TPE\text{-}NAG)_{10}$-*b*-$PSar_{53}$.

8. AIE property and self-assembly of P(TPE-NAG)-*b*-PSar

8.1 AIE property of P(TPE-NAG)-*b*-PSar

A strong absorption peak with a maximum around 312 nm was observed in the UV-vis absorption spectra of TPE-C_3OH and P(TPE-NAG)-*b*-PSar in DMF solution (Figure S14), which is a characteristic absorption of TPE group.[3, 12] The prepared P(TPE-NAG)-*b*-PSar block copolymers have numerous TPE groups pendant on the side chains. Their AIE properties are firstly studied before the self-assembly. With $P(TPE\text{-}NAG)_{25}$-*b*-$PSar_{46}$ as an example, a mixture of water and DMF with different water fraction (f_w), i.e. 0%, 30%, 60%, 90%, 99%, was added, respectively, to each of five flasks that contained a tiny volume of block copolypeptoids solution in DMF until a volume of 3 mL leading to 2.2×10^{-5} M polymer solution. As shown in Figure 2A, at f_w = 0, $P(TPE\text{-}NAG)_{25}$-*b*-$PSar_{46}$ is non-emissive because it is completely dissolved in DMF and the intramolecular rotation of TPE is active and serve as a relaxation channel for the excited states by UV illumination to deactivate.[13, 14] At f_w = 30% in DMF/H_2O mixture, the solution is "lit-up" with obvious fluorescence. The fluorescence intensity increases significantly as water fraction rising to 60% and 90%

in DMF/H_2O mixture. In nearly pure water (f_w = 99%), the aggregates of P(TPE-NAG)$_{25}$-*b*-PSar$_{46}$ show brightest AIE fluorescence (Figure 2A). In the aggregated state, the emission of TPE is induced by the effect of the restricted intramolecular rotation.[13, 14]

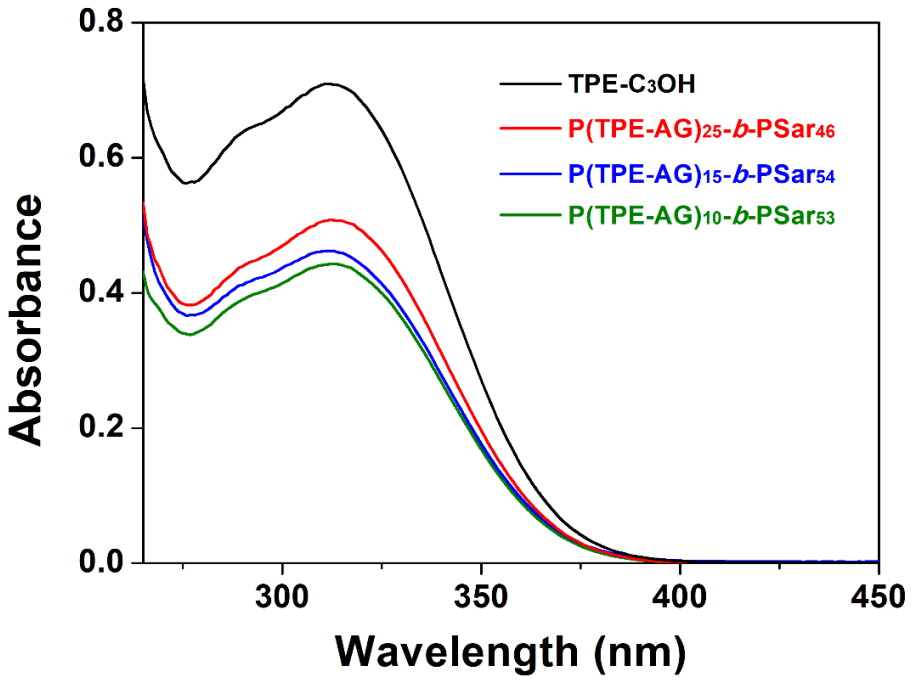

Figure S14. UV−vis absorption spectra of TPE-C_3OH, P(TPE-NAG)$_{25}$-*b*-PSar$_{46}$, P(TPE-NAG)$_{15}$-*b*-PSar$_{54}$, and P(TPE-NAG)$_{10}$-*b*-PSar$_{53}$ in DMF (concentration of TPE-C_3OH = 5 × 10^{-5} M and concentration of polymer = 1 × 10^{-5} M).

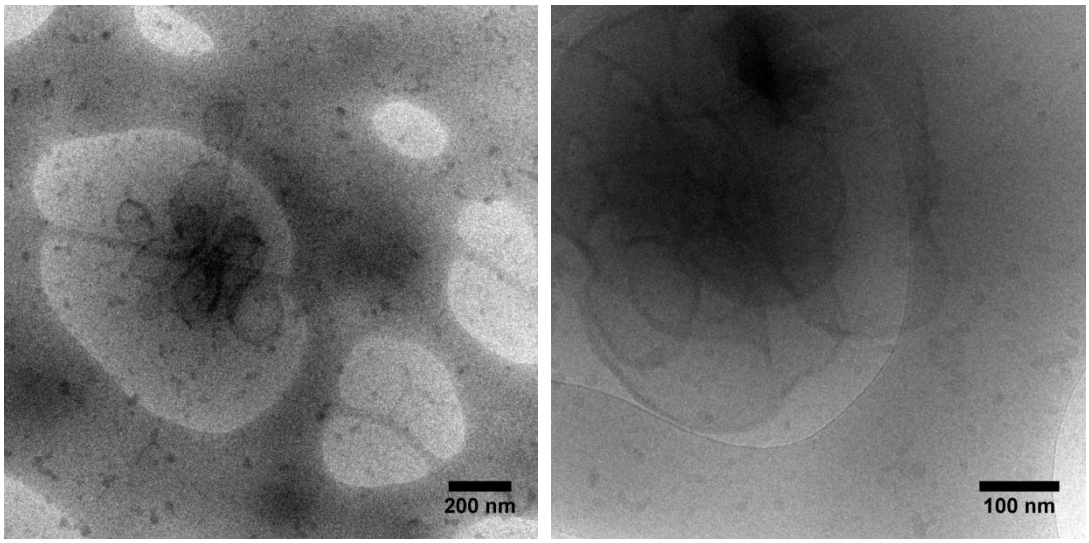

Figure S15. cryo-EM images of aggregates of P(TPE-NAG)$_{25}$-*b*-PSar$_{46}$ in DMF/H_2O mixture with water fraction at 99%.

8.2 Self-assembly of P(TPE-NAG)-*b*-PSar

Table S2. Sizes of nanoparticles self-assembled from P(TPE-NAG)-*b*-PSar by nanoprecipitation using DMF/water as co-solvents

Block copolypeptoids	$M_{n\ NMR}$[a] (kg/mol)	$Đ$[b]	f_{PSar} (%)[c]	*Peak 1*[d]		*Peak 2*[d]		$D_{cryo\text{-}EM}$ (nm)[e]	*Thickness* (nm)	*Quantum Yield (%)*[f]
				D_{DLS} (nm)	PDI	D_{DLS} (nm)	PDI			
$P(TPE\text{-}NAG)_{10}$-*b*-$PSar_{53}$	9.8	1.15	38	29	0.104	312	0.149	Micelles: 26 ± 4	-	27
$P(TPE\text{-}NAG)_{15}$-*b*-$PSar_{54}$	12.9	1.18	30	38	0.046	203	0.138	Micelles: 26 ± 4 Vesicle: 357 ± 82	8 ± 1	41
$P(TPE\text{-}NAG)_{25}$-*b*-$PSar_{46}$	18.3	1.16	18	136	0.040	804	0.123	Irregular vesicle: 227 ± 3 Spherical vesicle: 727 ± 154	10 ± 1	42

[a] Determined by NMR. [b] Determined by SEC. [c] The hydrophilic weight ratio (f_{PSar}) of the block copolypeptoids. [d] Average hydrodynamic diameters with intensity and PDIs determined by DLS. [e] Average diameters determined by analyzing 50 micelles or vesicles. [f] Measured by integrating sphere on PTI QM-40 system.

Note that despite the similarity between amphiphilic block copolymers and low molecular weight surfactants, amphiphilic block copolymers cannot form micelles or vesicles in thermodynamic equilibrium as their low-molecular-weight counterparts do. Most amphiphilic block copolymers are difficult to disperse in aqueous medium by themselves. Even starting with extremely low concentration, most amphiphilic diblock copolymers form quickly "frozen" aggregates in aqueous solution, *i.e.*, out-of-equilibrium structures unable to exchange free polymer chains ("unimers") within the experimental time scale. The key to controlling the dynamics of self-assembly of amphiphilic block copolymers in a selective solvent (here water) is the interfacial tension of core-forming block with the solvent.[15] This interfacial tension is normally very high for most of amphiphilic block copolymers. P(TPE-NAG)-*b*-PSar studied here are the case. Addition of a nonselective co-solvent to the aqueous solution is one of the strategies to reduce the interfacial tension between the hydrophobic block and aqueous solution and thus to promote unimer

exchange.[15, 16] In addition, the details of self-assembling process (the addition order of organic solvent and water, the speed of the solvent addition, the concentration, etc.) play also important role in the formation of nanostructures. We found in the standard AIE test that the quick addition of water into the DMF solution of P(TPE-NAG)$_{25}$-*b*-PSar$_{46}$ led to a few of very big and poorly defined vesicles (Figure 2D, Figure S15). Therefore, we used then a nanoprecipitation method with DMF/water as co-solvents and a slow water addition process to self-assemble P(TPE-NAG)-*b*-PSar in a controlled way.

The nanoparticles were prepared following a classical nanoprecipitation method.[3] As an example, P(TPE-NAG)$_{25}$-*b*-PSar$_{46}$ (2.0 mg) was dissolved in 1 mL of DMF. A total volume of 2 mL of deionized water was injected slowly at the rate of 2.5 μL/min with slight shaking. The whole process of nanoprecipitation was carried out at room temperature. The obtained turbid mixtures were then dialyzed against water for 3 days to remove the DMF using a Spectra/Por regenerated cellulose membrane with a molecular weight cutoff (MWCO) of 3500 Da.

As for the sizes and size distributions, the results obtained from cryo-EM and DLS (Table S2) are coherent, but not exactly the same. There are two reasons. Firstly, the DLS measured the hydrodynamic diameters of Z-average (with intensity profile, Figure 3A-C) or of number average (with number profile, Figure 3D-F), while cryo-EM measured number average diameters (without hydrophilic PSar corona part) over 50 nanoparticles for each population. Secondly, DLS measured sample in bigger volume with better statistical representation, while cryo-EM measured only the tiny quantity of aliquot trapped on the cryo-EM grid (where big objects can aggregate and produce thick ice, making them no longer be possible to be observed). Since the two populations in each polymer self-assemblies are well distinguished in DLS curves, we can separate them by filtration and obtain the wanted nanoparticles for future applications, for example, AIE polymer micelles with diameter around 30 nm in the case of P(TPE-NAG)$_{10}$-*b*-PSar$_{53}$ and AIE polymersomes with diameter of 100 – 200 nm in the case of P(TPE-NAG)$_{25}$-*b*-PSar$_{46}$.

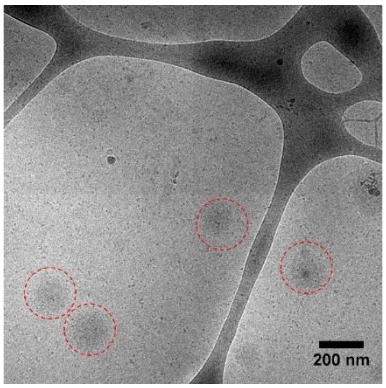

Figure S16. cryo-EM image of nanoparticles in water formed by P(TPE-NAG)$_{10}$-*b*-PSar$_{53}$. The red dashed circles refer to the aggregates of micelles.

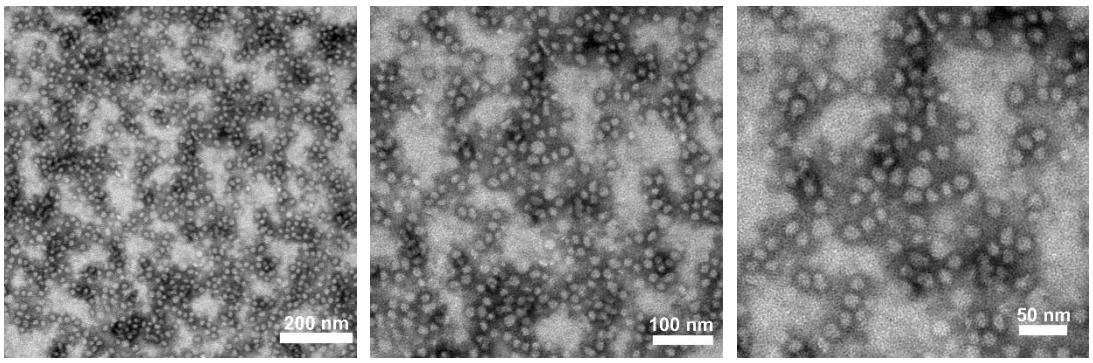

Figure S17. TEM images of micelles formed by P(TPE-NAG)$_{10}$-*b*-PSar$_{53}$ (f_{PSar} = 38%).

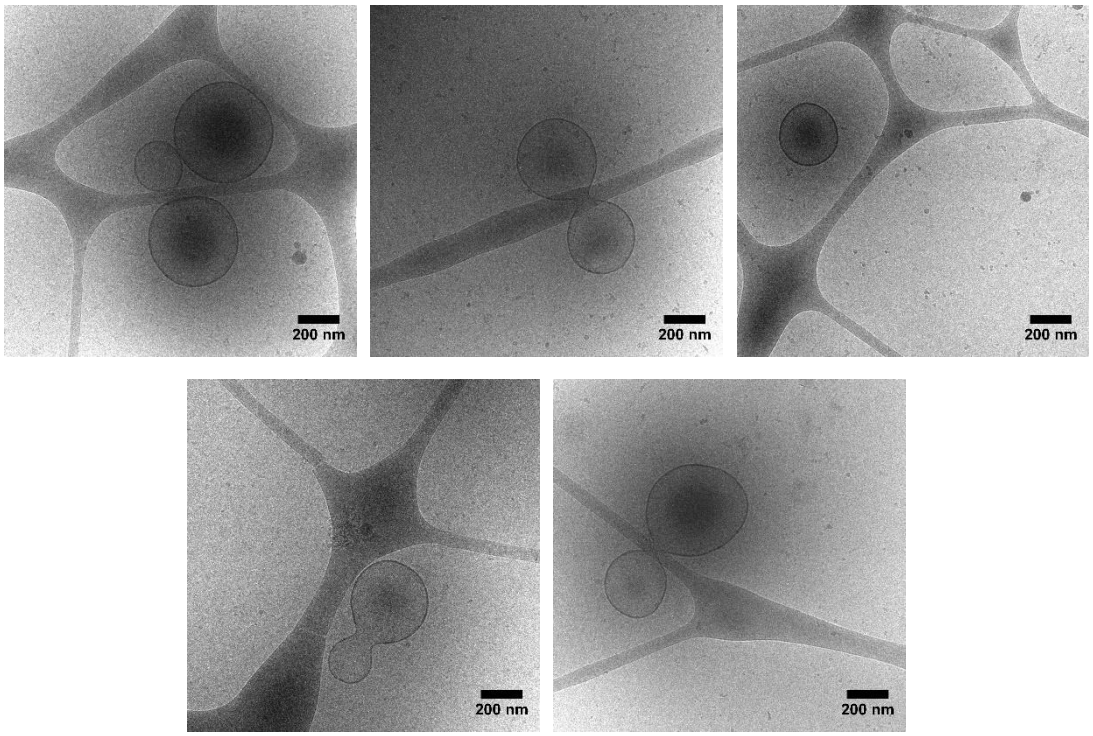

Figure S18. cryo-EM image of nanoparticles in water formed by P(TPE-NAG)$_{15}$-*b*-PSar$_{54}$ (f_{PSar} = 30%).

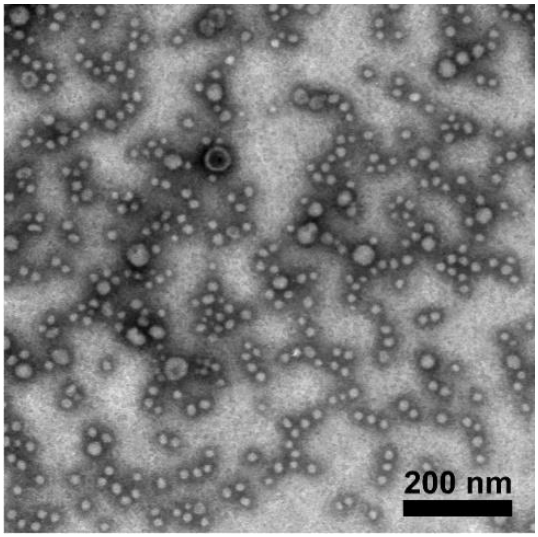

Figure S19. TEM images of nanoparticles formed by P(TPE-NAG)$_{15}$-*b*-PSar$_{54}$ (f_{PSar} = 30%).

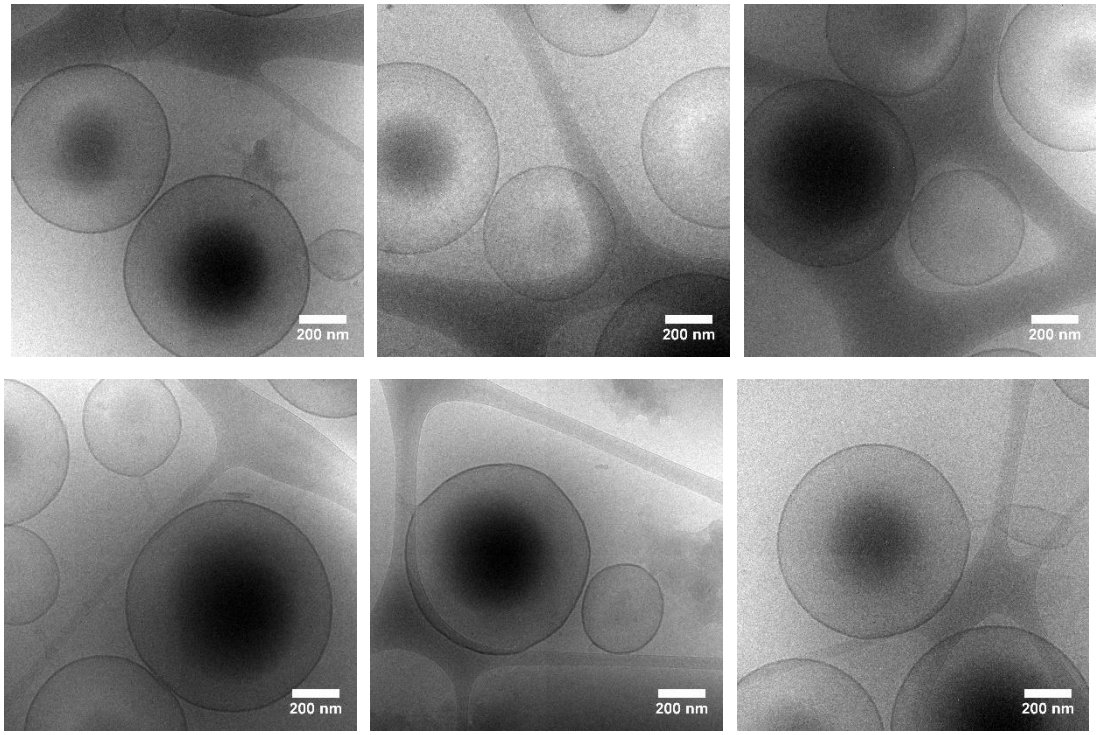

Figure S20. cryo-EM image of polymersomes in water formed by P(TPE-NAG)$_{25}$-*b*-PSar$_{46}$ (f_{PSar} = 18%).

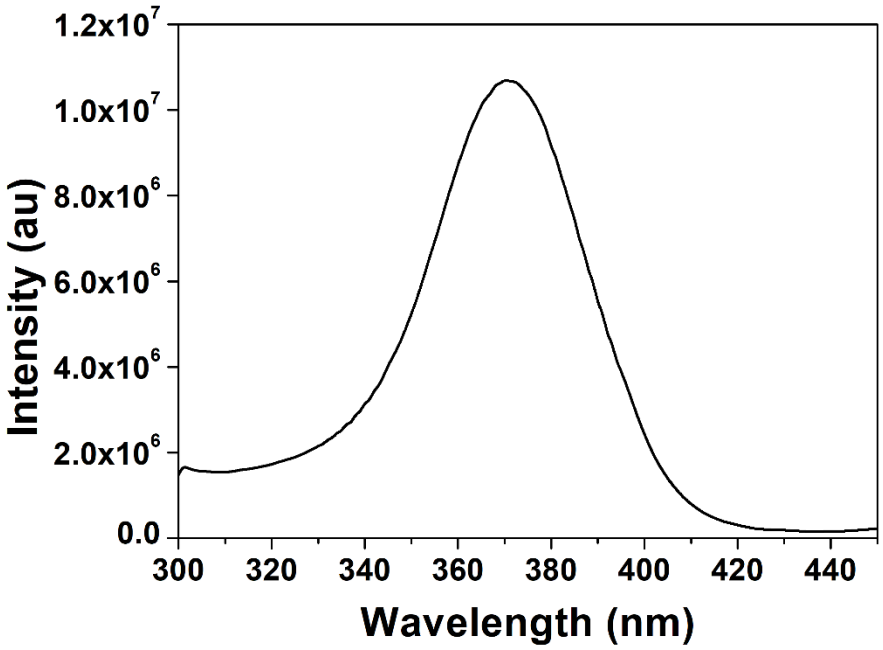

Figure S21. Excitation spectrum of P(TPE-NAG)$_{25}$-*b*-PSar$_{46}$ polymersomes in water. (Concentration: 0.4 mg/mL; emission wavelength: 471 nm).

9. Cytotoxicity Assay

Human vein endothelial cells (ECs) were purchased from the Center for Typical Culture Collection, Chinese Academy of Sciences (Shanghai, China). Cells were maintained in high-glucose DMEM (Gibco), supplanted with 10% fetal bovine serum (FBS, Sijiqing Co., Ltd., Hangzhou, China), 100 μg/mL penicillin, and 100 μg/mL streptomycin and cultured at 37 °C in a 5% CO_2 humidified environment. Cells were plated in a 96-well plate and cultivated to over 80% confluence. The medium was replaced with fresh medium containing varying concentrations of different P(TPE-NAG)-*b*-PSar nanoparticles. After 24 h of incubation, the cells were carefully washed with PBS to remove free nanoparticles and the cell viability was quantified using the MTT assay.[17-19] The viability of untreated cells was denoted as 100%.

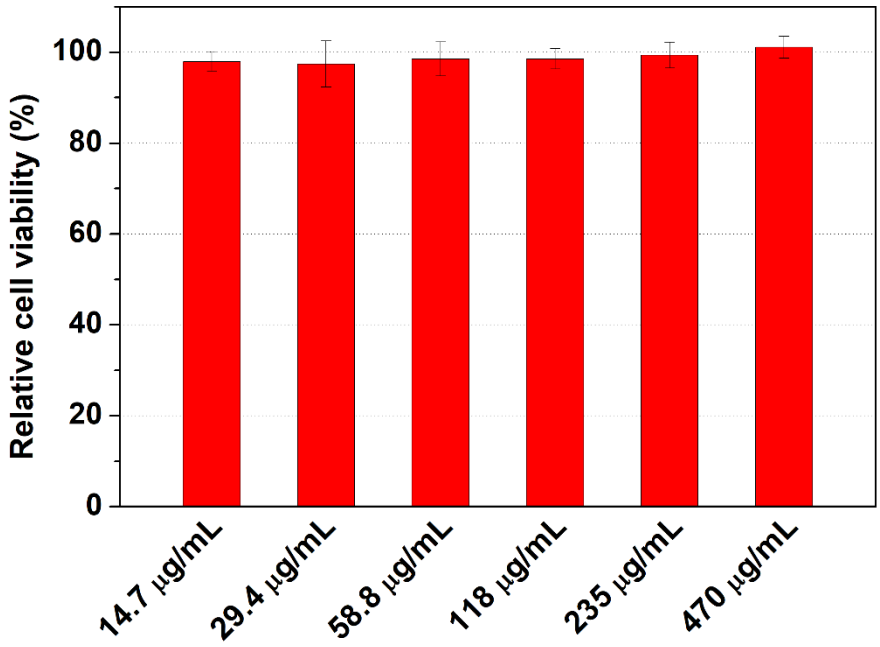

Figure S22. Relative cell viability of P(TPE-NAG)$_{10}$-*b*-PSar$_{53}$ nanoparticles for human vein endothelial cells after 24 h incubation at a concentration of 14.7 μg/mL, 29.4 μg/mL, 58.8 μg/mL, 118 μg/mL, 235 μg/mL and 470 μg/mL, respectively.

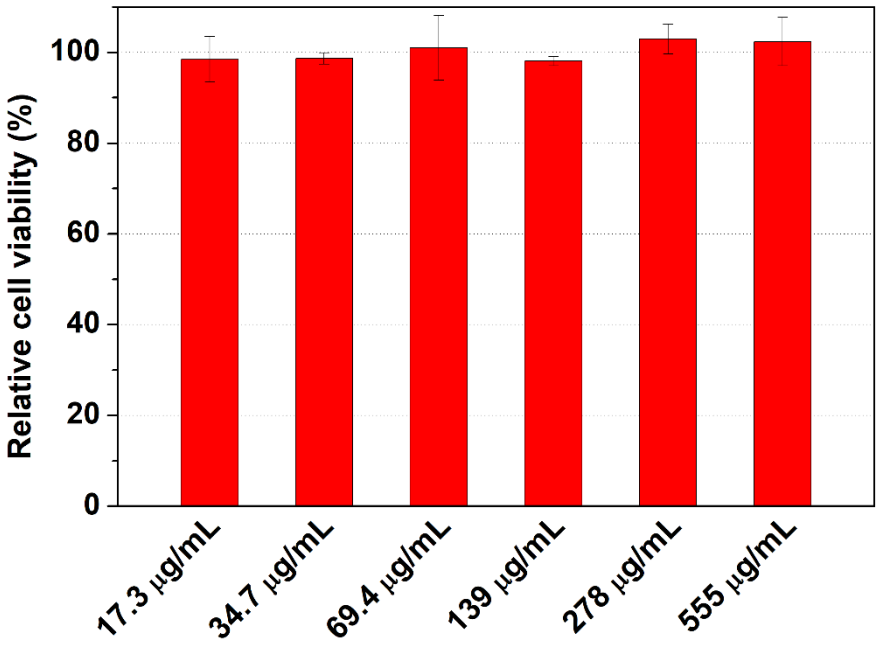

Figure S23. Relative cell viability of P(TPE-NAG)$_{15}$-*b*-PSar$_{54}$ nanoparticles for human vein endothelial cells after 24 h incubation at a concentration of 17.3 μg/mL, 34.7 μg/mL, 64.9 μg/mL, 139 μg/mL, 278 μg/mL and 555 μg/mL, respectively.

Reference

1 X. F. Tao, C. Deng and J. Ling, *Macromol. Rapid Commun.*, 2014, **35**, 875-881.

2 X. F. Tao, B. T. Zheng, H. R. Kricheldorf and J. Ling, *J. Polym. Sci., Part A: Polym. Chem.*, 2017, **55**, 404-410.

3 N. Zhang, H. Chen, Y. Fan, L. Zhou, S. Trepout, J. Guo and M.-H. Li, *ACS Nano*, 2018, **12**, 4025-4035.

4 H. Zhou, J. Li, M. H. Chua, H. Yan, B. Z. Tang and J. Xu, *Polym. Chem.*, 2014, **5**, 5628-5637.

5 L. Guo, S. H. Lahasky, K. Ghale and D. H. Zhang, *J. Am. Chem. Soc.*, 2012, **134**, 9163-9171.

6 X. F. Tao, J. W. Du, Y. X. Wang and J. Ling, *Polym. Chem.*, 2015, **6**, 3164-3174.

7 J. W. Robinson and H. Schlaad, *Chem. Commun.*, 2012, **48**, 7835-7837.

8 C. Xing, Z. Shi, J. Tian, J. Sun and Z. Li, *Biomacromolecules*, 2018, **19**, 2109-2116.

9 C. Fetsch, A. Grossmann, L. Holz, J. F. Nawroth and R. Luxenhofer, *Macromolecules*, 2011, **44**, 6746-6758.

10 A. Li, L. Lu, X. Li, L. L. He, C. W. Do, J. C. Garno and D. H. Zhang, *Macromolecules*, 2016, **49**, 1163-1171.

11 A. Birke, J. Ling and M. Barz, *Prog. Polym. Sci.*, 2018, **81**, 163-208.

12 D. Zhang, Y. Fan, H. Chen, S. Trépout and M.-H. Li, *Angew. Chem., Int. Ed.*, 2019, **58**, 10260-10265.

13 R. T. K. Kwok, C. W. T. Leung, J. W. Y. Lam and B. Z. Tang, *Chem. Soc. Rev.*, 2015, **44**, 4228-4238.

14 J. Mei, N. L. C. Leung, R. T. K. Kwok, J. W. Y. Lam and B. Z. Tang, *Chem. Rev.*, 2015, **115**, 11718-11940.

15 T. Nicolai, O. Colombani and C. Chassenieux, *Soft Matter*, 2010, **6**, 3111-3118.

16 L. Zhang and A. Eisenberg, *Macromol. Symp.*, 1997, **113**, 221-232.

17 C. Bi, J. Chen, Y. Chen, Y. Song, A. Li, S. Li, Z. Mao, C. Gao, D. Wang, H. Mohwald and H. Xia, *Chem. Mater.*, 2018, **30**, 2709-2718.

18 G. Yu, S. Yu, M. L. Saha, J. Zhou, T. R. Cook, B. C. Yung, J. Chen, Z. Mao, F. Zhang, Z. Zhou, Y. Liu, L. Shao, S. Wang, C. Gao, F. Huang, P. J. Stang and X. Chen, *Nat. Commun.*, 2018, **9**, 4335.

19 T. Jiang, J. Zhao, S. Yu, Z. Mao, C. Gao, Y. Zhu, C. Mao and L. Zheng, *Biomaterials*, 2019, **188**, 130-143.